ARTICLE TYPE

www. rsc.org/xxxxxx | XXXXXXXX

Thermoresponsive self-assembled NiPAm-zwitterion copolymers

Ya Zhao,[a] **Tao Bai,**[b] **Qing Shao,**[b] **Shaoyi Jiang,**[b] **and Amy Q. Shen**[a,c*]

Zwitterionic polymers are well known for their non-fouling properties due to their unique pendant side chain structures. In this work, we incorporated temperature-responsive *N*-isopropylacrylamide (NiPAm) with zwitterionic monomers (Carboxybetaine methacrylate (CBMA) and Sulfobetaine methacrylate (SBMA)), and synthesized statistical copolymers poly(NiPAm-*co*-CBMA) and poly(NiPAm-*co*-SBMA). Above the low critical solution temperature (LCST), a clear sol-gel transition was observed, accompanied by an increase in turbidity and elastic modulus in the copolymer solution. The self assembly and thermoresponsive properties of these statistical copolymers under large strains and different temperatures were characterized by UV-visible spectroscopy, dynamic light scattering, and rheological characterizations. We showed that poly(NiPAm-*co*-CBMA) copolymers consisted both mechanically and thermally reversible networks, favoring them as reusable and biocompatible elastic materials. As a comparison, incorporating SBMA with NiPAm inhibited the thermo-sensitive and viscoelastic features from the pure NiPAm based polymer, causing a delayed LCST and weakened viscoelastic response in poly(NiPAm-*co*-SBMA) copolymers at both room and body temperatures. Our work demonstrates that CBMA monomers in poly(NiPAm-*co*-CBMA) copolymer act as stronger ionic bridges to form elastic networks when compared with poly(NiPAm-*co*-SBMA) copolymer. As a result, poly(NiPAm-*co*-CBMA) possess both non-fouling and thermo-sensitive features, without compromising its mechanical properties.

1 Introduction

Zwitterionic polymers such as carboxybetaine methacrylate (CBMA), sulfobetaine methacrylate (SBMA), and phosphorylcholine based polymers, have been used to synthesize superhydrophilic and ultra low fouling biomaterials[1–4]. Commercially available low fouling nonionic polyethylene glycol (PEG) resists nonspecific protein adsorption via hydration forces, which are formed between hydrogen bonds and water molecules. However, PEG has been shown to interact with hydrophobic surfaces that can lead to oxidation of a substrate[5]. Zwitterionic based materials, with their strong intramolecular and intermolecular electrostatic interactions, can bind water molecules strongly and form electrostatically induced hydration[6–8], which resists nonspecific protein adsorption over the long run. In addition, some zwitterionic monomers can be functionalized with different elements, enabling the coated surface or bulk materials with ultra-nonfouling features. For example, SBMA can be attached onto hydrophobic substrates via sulfobetaine-hydrophobic bonds to exhibit fouling resistances. CBMA coated surface showed small absorbance of proteins (i.e., < 0.3 ng/cm^2 of proteins from 100% blood plasma or serum)[9–11], and low cell adhesion (i.e. of COS-7 cells)[12]. Compared with SBMA, CBMA has a similar molec-

ular structure but contains a weakly acidic carboxyl group. As a result, CBMA can be functionalized more easily with higher surface packing density[13]. Furthermore, the structure of carboxyl groups in CBMA is similar to that of glycine betaine (see Fig. 1), which is one of the compatible solutes vital to the osmotic regulation of living organisms. More recently, CBMA based hydrogels have exhibited good resistance to form capsules for at least 3 months after subcutaneous implantation in vivo[12]. Therefore, synthesizing CBMA based biomaterials has been an active research area.

Thermoresponsive polymers have also attracted considerable interests owing to their reversible phase transition behavior at lower critical solution temperature (LCST). To extend the application of zwitterionic materials, thermoresponsive statistical copolymers containing zwitterionic monomers have been synthesized[14–19]. Poly (*N*-isopropylacrylamide) (PNiPAm) is a thermo-sensitive polymer that is synthesized from *N*-isopropylacrylamide (NiPAm) monomers (see Fig. 1). PNiPAm exhibits a miscible to immiscible phase transition at lower critical solution temperature (LCST)[14–16,20] around 32 °C. The thermoresponsive PNiPAm can repeatedly swell and shrink when the temperature goes below and above LCST[14,20]. When the temperature exceeds its LCST, PNiPAm becomes dehydrated with broken bonds between hydrogen-polymer chains and coils of its hydrophobic tails, accompanied by an abrupt phase transition due to globular structural formation[14,20,21]. The hydrodynamic radius of the globular structure and the structure evolution under external con-

a Department of Mechanical Engineering, University of Washington, Seattle
b Department of Chemical Engineering, University of Washington, Seattle
c Micro/Bio/Nanofluidics Unit, Okinawa Institute of Science and Technology, Okinawa, Japan; E-mail: amy.shen@oist.jp

ditions can be detected by static and dynamic light scattering measurements [20,22,23]. By varying the hydrophobic and hydrophilic sequences in the diblock and triblock architectures (i.e, ABA block or BAB block), morphologies with core-shell [24], flower like, and interconnected micelles and networks [25–28] can be formed in thermoresponsive diblock and triblock copolymers containing PNiPAm. The hydrophobic and hydrophilic sequences are also switchable under different thermal conditions. For example, PNiPAm becomes hydrophobic above LCST with coil-to-globule transition, but can reverse back to be hydrophilic and soluble in water when the temperature goes below its LCST.

Different from thermoresponsive PNiPAm with LCST, most zwitterionic polymers exhibit an upper critical solution temperature (UCST), with an enhanced solubility in aqueous solutions with increasing temperatures [17,23,29]. For example, below its UCST, PolySBMA synthesized from SBMA monomers would precipitate in water due to the collapse of zwitterionic coils [17,23,29]. However, the zwitterionic chains become hydrophilic when the temperature increases above its UCST, becoming soluble in an aqueous solution. Combining segments of the zwitterionic polymers and thermo-responsive PNiPAm showed dual temperature sensitivity corresponding to the UCST of zwitterionic monomers and the LCST of PNiPAm [17,27,29–33]. For example, Lowe et al. [29] synthesized diblock copolymer from NiPAm with ammoniopropane sulfonate (SPP) by atom transfer radical polymerization (ATRP) method, while Arotana et al. [34] synthesized diblock copolymer from NiPAm with SBMA by reversible addition fragmentation chain transfer (RAFT) technique. Both research groups observed that above the LCST of PNiPAm (~ 32 °C), the copolymer formed colloidal aggregates with hydrophobic coils from PNiPAm being surrounded by SBMA or SPP hydrophilic groups. Below the UCST of SBMA (27 °C) or SPP, reversed aggregates were formed from collapsed SBMA or SPP coils that were solubilized by PNiPAm groups.

These zwitterionic and NiPAm based copolymers have shown great advantages for biological in-vivo applications with their dual non-fouling and thermo-responsive features. In more recent work, the biocompatible property of a zwitterionic-based statistical copolymer was evaluated as antifouling and bioinert coating for biomedical devices, by forming a biomembrane-alike film to resist biological interactions in-vivo [35–37]. Even though it is easier to control the mass distribution and segment architecture in block copolymers [38], the block copolymers are easily micellized in aqueous solution, which renders the contact between hydrophobic components and the substrate and has an adverse effects on the coating quality [37]. As a comparison, statistical copolymer architectures are superior when the solvent is suitable for both segments. Hence, the statistical copolymers are more likely to form a stable and uniform coating on a large selection of sub-

strate in the context of biomaterials. For example, Chang et al. [17] studied copolymers synthesized from NiPAm and SBMA monomers by random copolymerization and extended the bioadhesive application of poly(NIPAAm-*co* - SBMA) [39]. They showed how the UCST and LCST of the copolymer systems were affected by changing the molar percentage of the two monomers, ionic environment, and their mass concentrations. In addition, micelles formed below the UCST of zwitterionic monomers and above the LCST of PNiPAm exhibit different aggregation behaviors and thermal responses with different ionic strength and the segment mobility in the copolymer system [30,31]. Combing zwitterionic and thermoresponsive features, Obiweluozor et al. [40] recently investigated the veiscoelastic behavior of a NiPAm-zwitterion copolymer solution as a function of ionic strength in the presence of different ions. They demonstrated that the inter-/intramolecular electrostatic crosslinks among the sulfobetaine chain could be effectively manipulated by the amount of low-molecular-weight ions.
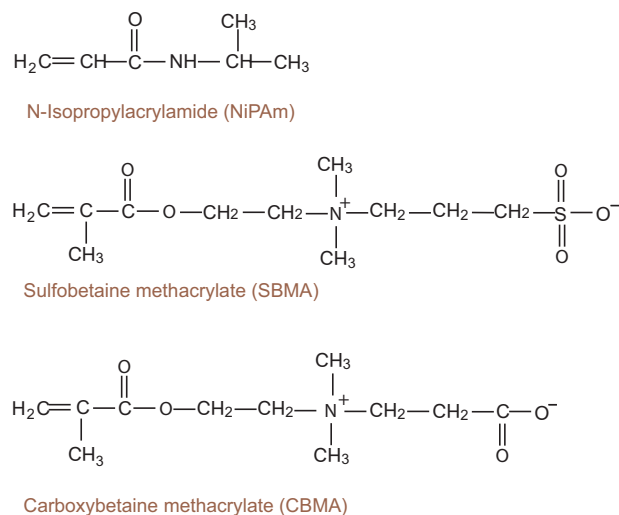

Fig. 1 Chemical structures of NiPAm, SBMA, and CBMA monomers.

Motivated by the dual temperature responses for PNiPAm and zwitterionic polymers, the goal of this work is to synthesize self-assembled statistical copolymers that retain relatively strong mechanical properties under large strains with varying temperature conditions, while possessing both non-fouling and thermoresponsive features. In particular, we focus on two statistical copolymers of poly(NiPAm-*co*-CBMA) and poly(NiPAm-*co*-SBMA), synthesized from NiPAm and zwitterionic monomers (CBMA and SBMA), with different weight ratios of zwitterionic to NiPAm monomers. We performed detailed material characterizations of copolymers by conducting UV-visible spectroscopy, dynamic light scattering, and rheological measurements under different temperatures and large

amplitude oscillatory shear, illustrating thermo-sensitive self-assembly/disassembly of copolymer aggregates in an aqueous solution. The capacity of elastic recovery of the assembled aggregates under alternating temperatures and strains was also assessed and compared in poly(NiPAm-*co*-CBMA) and poly(NiPAm-*co*-SBMA) systems.

2   Materials and Methods

2.1   Materials Preparation

2-Carboxy-N,N,-dimethyl-N-(2′–(methacryloyloxy) ethyl) ethanaminium inner salt (carboxybetaine methacrylate, CBMA) was synthesized using an existing protocol ($> 99\%$ purity)[2]. Both [2-(Methacryloyloxy)ethyl]dimethyl(3-sulfopropyl)-ammonium hydroxide (sulfobetaine methacrylate, SBMA) and N-Isopropylacrylamide (NiPAm) ($> 97\%$ purity) were purchased from Sigma-Aldrich (Saint Louis, MO) and used as received. The chemical structure of these monomers are shown in Fig. 1. Ammonium persulfate (APS), $N,N,N′,N′$-Tetramethylethylenediamine (TEMED) from Bio-Rad Laboratories (Hercules, CA) were used as received.

We dissolved CBMA (or SBMA) and NiPAm monomers at different mass ratios in DI water, as shown in Table 1. The copolymerization of poly(NiPAm-*co*-C(S)BMA) was initiated by using 2 wt% of APS and 0.2 wt% of TEMED in total monomers, in a nitrogen atmosphere. The solution was stirred at room temperature for 24 h with the polymerization process illustrated in Fig. 2.

After polymerization, the resulting solutions were stored in a membrane tubing in DI water for at least 24 h to remove the residual unpolymerized chemicals. Subsequently the membrane tubing containing the solution was connected to a freeze dryer (FreeZone 1 Liter, Labconco) for at least 48 h to yield white powders. Finally, synthesized copolymers in powder form were dissolved in deionized water at 8 wt% to prepare for stock copolymer solutions at pH = 7.0. Serving as a control for comparison purposes, PNiPAm, polySBMA, and poly-CBMA in powder form were also synthesized by following the same protocol with individual NiPAm, SBMA, or CBMA monomers as reacting components. The molecular weights of polymers (PS3_1, PS5_1, PC3_1, PC3_1) were determined by gel permeation chromatography (GPC) on a Waters Alliance 2695 system fitted with a Phenomenex BioSep-SEC-s2000 column.

2.2   Material composition characterizations

We first characterized the structure of all the PC and PS copolymers by obtaining their proton nuclear magnetic resonance (^{1}H NMR) spectra by using a Bruker AV500 series spectrometer with a 1H frequency at 499.956 MHz and D$_2$O
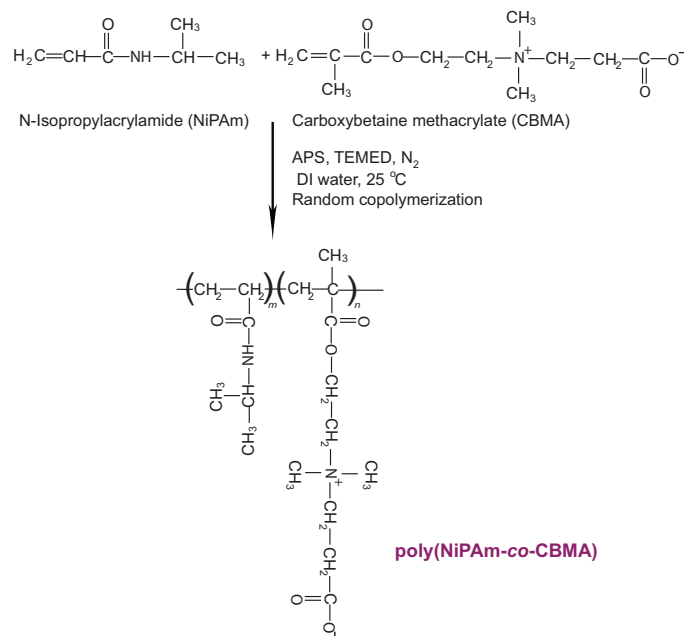

Fig. 2 Illustration of copolymerization process to synthesize statistical copolymer poly(NiPAm-*co*-CBMA). Similar copolymerization process also applies to the statistical copolymer poly(NiPAm-*co*-SBMA).

as the lock solvent. The composition of the PS copolymers was estimated from the relative area of $(CH_3)_2N^+$ proton resonance of the polySBMA side group at $\delta = 3.2$ ppm. The composition of the PC copolymers was estimated from the relative area of $(CH_3)_2N^+$ proton resonance of the polyCBMA side group at $\delta = 3.16$ ppm. The composition of the polyNIPAAm was estimated from the relative area of the methyl proton resonance of the polyNIPAAm isopropyl group at $\delta = 1.1$ ppm. See more details in the supporting information. The molar ratio for four copolymers is listed in Table 1.

Gel Permeation Chromatography (GPC) experiments were then conducted on an Agilent 1260 system with refractive index (RI) and multiple-angle light scattering (MALS) detectors from Wyatt Technology. The copolymers were dissolved in Deionized water to a concentration of 5 mg/mL and separated on an Agilent PL Aquagel-OH 20 column with a flow rate of 1 mL/min and DI water as the mobile phase. Polydispersity index (PDI) values were calculated from the collected RI and MALS data using the ASTRA software developed by Wyatt Technology, and molecular weight (Mw) was calculated from a polyethylene glycol (PEG) standard curve. Each polymer was separated and analyzed three times under the same conditions, the Weight-average molecular weights (Mw) and molecular weight distributions (Mw/Mn) for 4 different copolymers were listed in Table 1.

Based on NMR and GPC measurements, we detect slight

Table 1 Chemical compositions and characteristic Data of Poly(NiPAm-*co*-C(S)BMA) Statistical Copolymers.

Materials[a]	Reaction ratios (wt %)		Composition ratios (mol %)		Copolymers characterization		Critical temperature (°C)
	S(C)BMA	NiPAm	polyS(C)BMA	PNiPAm	Mw (g/mol) [b]	Mw/Mn[c]	LCST[d]
PC3_1	166.7	500	11.7	88.3	42535	1.172	34
PC5_1	100	500	6.25	93.97	44835	1.298	34
PS3_1	166.7	500	13.3	86.7	42838	1.257	36
PS5_1	100	500	8.1	91.9	46018	1.316	34

[a] The copolymer labels in the first column are based on the reaction mass ratios of NiPAm and C(S)BMA monomers used, with fixed NiPAm monomer mass amount of 500 mg and different mass of C(S)BMA monomers. For example, PC5_1 is synthesized from NiPAm and CBMA monomers with a mass ratio of 5:1; PS3_1 is synthesized from NiPAm and SBMA monomers with a mass ratio of 3:1. [b] Weight-average molecular weights (Mw) and [c] molecular weight distributions (Mw/Mn). [d] LCST were determined by the absorbance data on a UV-visible spectrophotometer.

differences in the molecular compositions percentages of PC and PS copolymers used. However, all samples exhibited a similar average molecular weight of about 42∼46 kDa and a narrow molecular weight distribution (Mw/Mn = 1.1–1.3).

2.3 UV-Visible Spectroscopy

The phase transition behavior of the copolymer solutions was characterized by using a Varian Cary 5000 UV-Vis-NIR Spectrophotometer coupled with a temperature controller at 1 °C/min under temperature range of 25 °C to 40 °C. The soluble to insoluble phase transition was recorded as a function of absorbance intensity versus temperature. In order to obtain the absorbance intensity at the instrument measurable range, all the stock copolymer solutions were diluted 10 times to a concentration of 0.8 wt%. A wave spectrum scan from 200 nm to 800 nm was performed first to identify the peak absorbance at each individual temperature in the range of 25 °C to 40 °C. The peak absorbance intensity was then subtracted from the spectrum scan under different temperatures and plotted as a function of temperature. The LCST (or UCST) of the copolymer (or polymer) were determined by referring to the temperature where the maximum slope of the absorbance change occurred and the LCST for 4 different copolymers were listed in Table 1.

2.4 Dynamic Light Scattering

Dynamic light scattering (DLS) measurements were conducted by a light scattering apparatus equipped with a He-Ne laser (Zetasizer Nano ZS, Malvern). The copolymer solutions were prepared by dissolving 0.8 wt% copolymers in DI water with pH = 7.0, and placed in a reduced volume polystyrene cuvette. The time correlation functions measured by DLS were analyzed by a Laplace inversion program (CONTIN)[41–43]. Experiments were carried out in a temperature range from 25 °C to 40 °C, at the scattering angle of 173° and the wavelength at 633 nm under vacuum setting. At each temperature the samples were equilibrated for 20 min before each measurement.

2.5 Bulk Rheometry

The viscoelastic properties of the stock copolymer solutions were characterized by using a stress controlled rheometer (Malvern Kinexus Pro rheometer). All measurements were performed by using a stainless steel cone and plate geometry (40 mm in diameter and a cone angle of 2°) with a truncation gap of 59 μm. A solvent trap was used to prevent drying effects. Oscillatory strain sweeps were first performed to determine the linear and nonlinear viscoelastic regime for each sample. To investigate the thermo-sensitivity of the copolymer solution, we performed oscillatory temperature sweep between 25 °C and 40 °C in the linear viscoelastic regime (with strain $\gamma = 1\%$ and frequency $f = 0.1$ Hz), during which, the elastic moduli G' and viscous moduli G'' were recorded and the sol-gel-sol transition was characterized.

To investigate the mechanical properties of the copolymer solution under thermal and mechanical stimulus, elastic moduli G' of the sample was measured as a function of time in the linear viscoelastic region ($\gamma = 1\%$ and $f = 0.1$ Hz for 10 min) before and after a large amplitude oscillation ($\gamma = 1000\%$ and $f = 0.1$ Hz for 4 min), under both room temperature (25 °C) and body temperature (37 °C). The sample was initially held at 37 °C, cooled to 25 °C, heated to 37 °C again with a ramp rate of 1 °C/min, with a 5 min isothermal hold between successive steps in the temperature cycle. Large strain ($\gamma = 1000\%$) and small strain ($\gamma = 1\%$) sweep were also carried out alternatively to characterize the mechanical stability of two copolymer solutions (PC3_1 and PS3_1) under body temperature 37 °C. All the measurements were performed three times to ensure data
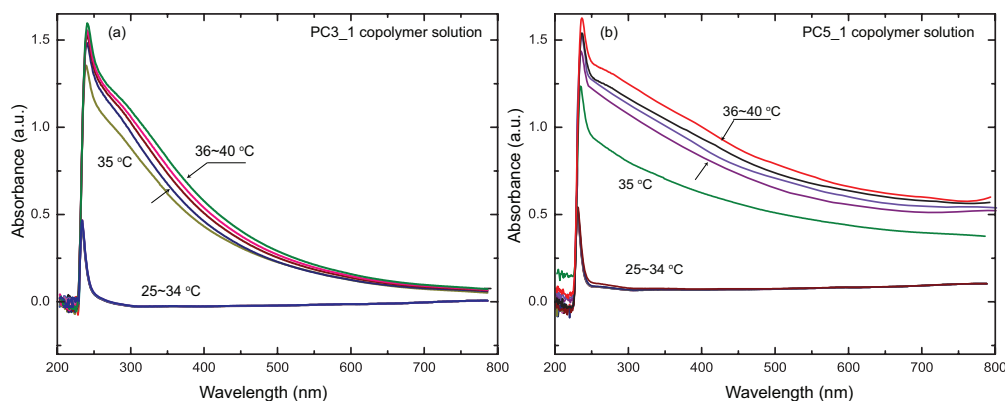
Fig. 3 Absorbance intensity as a function of UV scanning spectrum of (a) 0.8 wt% PC3_1 copolymer solution; (b) 0.8 wt% PC5_1 copolymer solution. The abrupt increase of the absorbance intensity corresponds to the phase transition in the copolymer solution, and the transition temperature corresponds to the LCST of PC3_1 and PC5_1.

reproducibility.

3 Results and Discussion

3.1 UV-vis spectroscopy

The temperature-dependent phase transition behavior of the copolymer solutions can be characterized by wavelength absorbance measurements by using UV-visible spectroscopy. Four zwitterionic based copolymers with different mass ratios of NiPAm monomers and CBMA (or SBMA) were prepared following the experimental procedure described in Materials and Methods (see Table 1). Stock copolymer solutions were diluted 10 times to a concentration of 0.8 wt% to obtain a measurable intensity range. A wave spectrum scan from 200 nm to 800 nm was performed first to identify the peak absorbance at each individual temperature in the range of 25 °C to 40 °C, as shown in Fig. 3 for PC copolymers and Fig. 4 for PS copolymers.

The maximum absorbance of both PC and PS copolymers occurred around 230 nm at 25 °C. Fig. 3 showed a noticeable increase of peak absorbance intensity when the temperature reaches beyond 35 °C for PC copolymers. The sharp increase in the absorbance intensity usually implies the emergence of broken hydrogen bonds and the collapse of hydrophobic polymer chains, leading to colloidal aggregates formation above its LCST, which is often accompanied by an increase of turbidity and precipitations, that can be visualized as milky and insoluble in the solution [14,17,23,39]. Similar phase transition temperature (around 35 °C) also occurred for PS5_1 as shown in Fig. 4(b), accompanied by an abrupt increase of the absorbance intensity around 35 °C. However, PS3_1 did not exhibit an abrupt temperature transition, instead displaying a gradual increase of absorbance intensity starting from 35 °C

(see Fig. 4(a)), implying the counter thermal effect caused by increasing amount of SBMA in the copolymer.

In order to identify LCST for PC and PS copolymers, the peak absorbance intensity value around 230 nm for each temperature was identified from the spectrum scan in Fig. 3 and Fig. 4, and plotted as a function of the temperature (see Fig. 5). The LCST can then be determined by referring to the temperature when the maximum slope of the absorbance change occurs. Similar procedure was used to capture the LCST of PNiPAm as a control study, shown as the dashed line in Fig. 5. PNiPAm at 0.8 wt% exhibited a LCST around 33 °C, which was consistent with existing reports [17]. A delay of LCST for both PC and PS copolymers compared with pure PNiPAm was observed. Similar phenomenon was reported for the copolymer poly(NiPAm-co-SBMA) with different molar ratios [17]. Chang et al. [17] proposed that when the molar ratio of the zwitterionic monomers to NiPAm increased in the copolymers, hydrophobic interactions between NiPAm chains became weaker. As a result, the required critical temperature had to increase to associate these chains before the formation of an insoluble phase.

In addition, the phase transition behavior was slightly different between the PC and PS copolymer solutions. Fig. 5 illustrated that higher weight percentage of SBMA synthesized in PS3_1 copolymer (green squares) apparently delayed the critical phase transition temperature in comparison to that of PS5_1 copolymer (purple squares). Increasing amount of sulfobetaine groups in SBMA (i.e., PS3_1 copolymer solution) contributed to an enhanced hydration capacity in the polymer chains, therefore, higher thermal energy was needed to overcome the repulsive forces between the hydration layers to collapse the NiPAm coils. However, the phase transition in PC5_1 and PC3_1 occurred around the same temperature
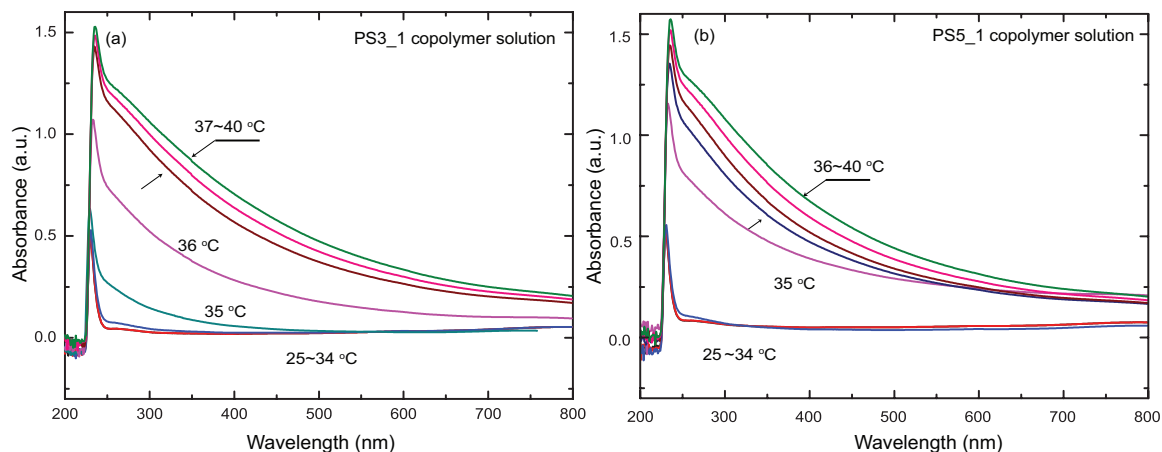
Fig. 4 Absorbance intensity as a function of UV scanning spectrum of (a) 0.8 wt% PS3_1 copolymer solution; (b) 0.8 wt% PS5_1 copolymer solution. The abrupt increase of the absorbance intensity corresponds to the phase transition in the copolymer solution, and the transition temperature corresponds to the LCST of PS3_1 and PS5_1.
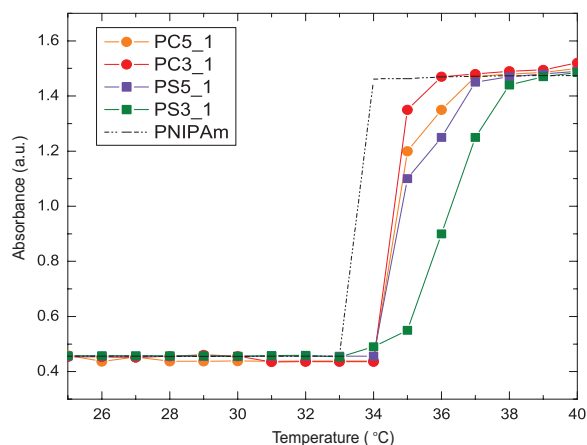

Fig. 5 Absorbance intensity as a function of temperature for 0.8 wt% PS and PC copolymer solutions, compared with 0.8 wt% PNiPAm solution. The LCST of the PS and PC copolymer was determined by referring to the temperature where the maximum slope of the absorbance change occurs.

Fig. 6 Absorbance intensity of polyCBMA and polySBMA solutions as a function of temperature at the polymer concentration of 0.8 wt%. The inset images show turbid polySBMA below its UCST and transparent state above its UCST, while polyCBMA maintains its transparent state during the entire temperature range. The gray area is the background of the cuvette.

at 34 °C. Since CBMA are only weakly affected by temperatures, incorporating CBMA with NiPAm did not counter affect the thermal sensitivities of NiPAm as much as SBMA did.

To investigate whether individual polyC(S)BMA is sensitive to the temperature effect, we synthesized polySBMA and polyCBMA with similar polymerization process. Again we dissolved 0.8 wt% of polyC(S)BMA in DI water and conducted absorbance measurements using UV-visible spectroscopy. Fig. 6 showed the intensity absorbance of polyS-BMA and polyCBMA from 5 °C to 40 °C. Similar to the
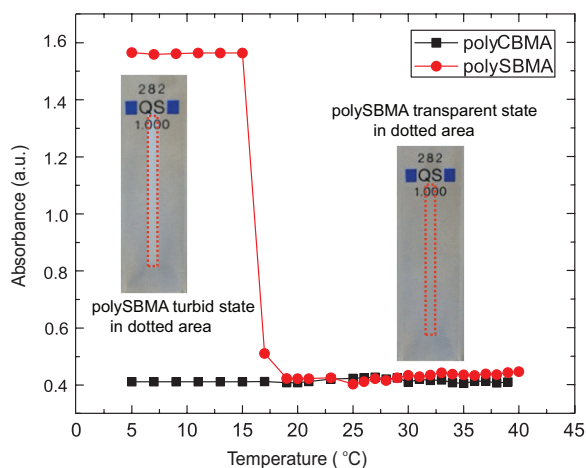
phase transition of PNiPAm above LCST, polySBMA (in red circles) showed a temperature dependent UCST behavior that had been commonly reported for zwitterionic polymers[17]. Below 15 °C, a typical coil-globule transition occurred initially, followed by chain aggregations due to the intermolecular interactions between the hydrophobic group exhibiting a sharp transition in the absorbance intensity. Hence, UCST of polyS-BMA can be considered around 15 °C for 0.8 wt% polyS-BMA solutions, at which temperature, polySBMA solutions
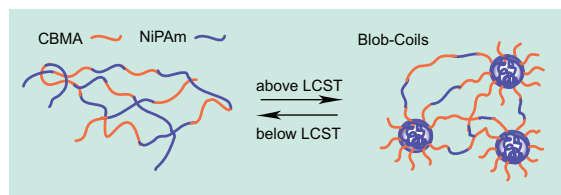
Fig. 7 Schematic illustration of the collapse of NiPAm coils in poly(NiPAm-*co*-CBMA) copolymer above the LCST of the copolymer.

showed turbidity as shown in the inset image. Interestingly, polyCBMA did not exhibit any sharp transition in its absorbance intensity between 5 °C to 40 °C (black symbols). This is consistent with our argument that the sulfobetaine group present in SBMA and its strong response to temperature is responsible for the different phase transition behaviors between poly(NiPAm-*co*-S(C)BMA) copolymers. Finally, since the weight percentage of C(S)BMA in our samples were relatively small in comparison to the NiPAm concentration, the UCST of copolymers were not observed even around 5 °C. As the main focus of this work is to distinguish the mechanical property difference between poly(NiPAm-*co*-CBMA) and poly(NiPAm-*co*-SBMA) copolymers, the subsequent studies mainly focused on the material characterizations at temperatures ranging from 25 to 40 °C.

3.2 Dynamic Light Scattering (DLS)

The copolymer solutions were prepared by dissolving 0.8 wt% copolymers in DI water and placed in a reduced volume polystyrene cuvette. Dynamic light scattering measurements were carried out in a temperature range from 25 °C to 40 °C, at the scattering angle of 173° and the wavelength at 633 nm under vacuum setting. Hydrodynamic radius R_h was plotted against temperature from DLS measurements for PC and PS copolymers, along with pure PNiPAm polymer as the control study.

The self-assembly of the thermoresponsive copolymers can also be identified by changes in the hydrodynamic radius R_h of the aggregates by using dynamic light scattering (DLS), when the thermally induced phase transition occurs in an aqueous solution (LCST, UCST, or both)[17,27,29–33], see schematics in Fig. 7. Below the LCST, both PNiPAm and C(S)BMA chains would extend in the aqueous solution. The hydrodynamic radius R_h of PNiPAm blobs would increase abruptly to the maximum value, reaching the LCST, corresponding to the formation of PNiPAm blobs. With further increasing temperatures, PNiPAm blobs would start to shrink and form smaller but dense globule, characterized by a gradual decrease in the hydrodynamic radius, see Fig. 8. A hysteresis between cooling (dashed curves with hollow symbols) and heating (solid

curves with filled symbols) processes was observed for the copolymers, see Fig. 8. Wu and Wang observed similar hysteresis behavior in the average radius of gyration and average hydrodynamic radius during the heating and cooling process in aqueous PNiPAm solutions[20]. They proposed that the coil-to-globule (heating) cycle led to "crumpled coil" state, while the globule-to-coil (cooling) transition led to "molten globule" state, with two states being thermodynamically stable. Similar arguments can be possibly applied to our copolymer system, originated from the polymerized zwitterionic chains.

By comparing Fig. 8(a) and Fig. 8(b), a noticeable difference in the R_h versus temperature trend was observed. For both PC5_1 and PC3_1 solutions, R_h peaked at LCST of the solution, followed by a decrease in R_h with further temperature increase. Similar trend in R_h of PNiPAm versus temperature (black dashed line) is observed in Fig. 8(a), but the magnitude of R_h in PNiPAm is higher than that of the PC copolymers. For both PC copolymer and PNiPAm solutions, at temperatures higher than LCST, PNiPAm globule kept on shrinking, leading to a decrease in R_h. In Fig. 8(b), the hydrodynamic radius R_h in PS5_1 were comparable with R_h of PNiPAm, but larger than R_h in PC5_1, possibly caused by stronger hydration layers formed around SBMA chains with increasing temperatures. For the PS copolymer solutions, the hydration layers formed by sulfobetaine chains in SBMA increased with increasing temperature and were also accompanied by stronger repulsive forces between the hydration layers, prompting elevated intramolecular forces to separate the hydrophilic coils on the surface. As a result, the hydrophobic PNiPAm blobs shrunk more significantly when being exposed to water in the PS copolymer solution, leading to a substantial decrease of R_h in PS5_1 ($\sim 33\%$) solution when compared with that of PC5_1 ($\sim 20\%$) solution. Moreover, our DLS measurements also revealed that weak intramolecular interactions between carboxyl groups in CBMA had less influence on the thermo-sensitivity of PNiPAm.

Finally, we observed that R_h of PS3_1 copolymer solution increased first but reached a plateau with further temperature increase, showing very different behavior from the PC and PS5_1 copolymer solutions. Compared with carboxybetaine groups present in PC3_1, which are weakly affected by temperatures, the thermal sensitivity of sulfobetaine chains in PS3_1 played an important role in the hydrodynamic radius transition and the balance of hydrophobic and hydrophilic interactions. This effect becomes more substantial with increasing amount of SBMA in the PS3_1 copolymer solution, where the globule and hydrophilic chain structures undergo a balance of intramolecular forces between PNiPAm and polySBMA chains. The PNiPAm chains with increasing hydrophobicity tried to collapse while the SBMA chains with increasing hydrophilicity tried to extend, leading to limited collapses of PNiPAm coils in PS3_1 solutions at higher temperatures.
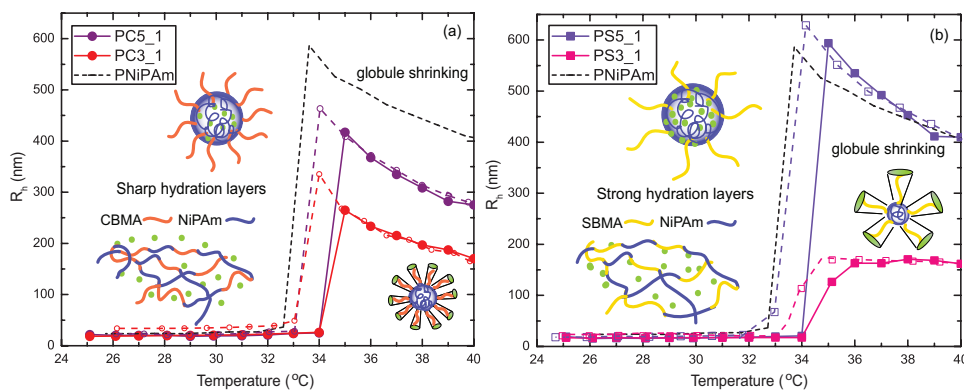
Fig. 8 Hydration radius R_h plotted against temperature from dynamic light scattering measurements for (a) 0.8 wt% PC copolymer solutions; (b) 0.8 wt% PS copolymer solutions. The dashed line corresponds to the hydration radius R_h of PNiPAm as a function of temperature. Single coil-blobs structure was shown to simplify the illustration
.The green dots represent water molecules. The cones around C(S)BMA chains represent hydration layers. Solid curves with filled symbols represent heating processes, while dashed lines with hollow symbols correspond to cooling processes.

These shrunk globule cores corresponded to a constant R_h at high temperatures, yielding the plateau behavior for PS3_1 during both heating (solid curve) and cooling process (dash curve). As a comparison, there were no increasing strong hydration layers formed in PC3_1, the transition trend of R_h is thus very similar to PC5_1 and PNiPAm.

3.3 Rheological characterizations

3.3.1 Oscillatory frequency sweep Oscillatory frequency sweep was performed under linear viscoelastic regime ($\gamma = 1\%$) and nonlinear viscoelastic regime ($\gamma = 1000\%$) for PS3_1 and PC3_1 at 25 °C and 37 °C, respectively (see Fig. 9). PC3_1 at 37 °C exhibited typical gel response at $\gamma = 1\%$, with G' being close to a constant and G'' curve was consistently lower than the G' curve throughout the entire frequency range (red symbols in Fig. 9(a)). However, at larger strain $\gamma = 1000\%$, PC3_1 showed viscoelastic response (blue symbols in Fig. 9(a)). At 25 °C shown in Fig. 9(c), PC3_1 solution displayed viscous dominated response at all frequency range, at both small and large strains. This observation is consistent with our speculation that PC3_1 solution does not contain self assembled aggregates at room temperature. The PS3_1 solution followed similar trend at different temperature and frequency ranges to those of PC3_1, but with a much lower value of both G' and G'' modulus (see Fig. 9(b) and (d)). In particular, the elastic modulus for the PS3_1 solution was too weak to be detected at 25 °C at large strain ($\gamma = 1000\%$).

3.3.2 Temperature sweep The sol gel transition behavior for all four copolymer solutions (PS3_1, PS5_1, PC3_1 and PC5_1) was characterized by a temperature sweep under small amplitude oscillations ($\gamma = 1\%$ and $f = 0.1$ Hz), with temperature varying from 25 to 40 °C, followed by cooling back to 25 °C, with a temperature ramp rate of 1 °C/min, as shown in Fig. 10.

For PC3_1 and PC5_1 solutions, viscous modulus G'' (in dashed curves) was more dominant than plateau modulus G' (in solid curves) at temperatures below 33 °C, see Fig. 10. After reaching the phase transition temperature around 34 °C (close to the LCST of the copolymer), G' (solid curves) became more dominant, which is consistent with our DLS characterizations (Fig. 8), showing gel-like network formation at temperatures above LCST.

Both PC3_1 and PC5_1 solutions showed a clear sol-gel transition with a maximum G' of 100 Pa and 200 Pa respectively, see purple solid curve and red solid curve in Fig. 10. The higher weight ratio of PNiPAm in PC5_1 favored more PNiPAm blobs to form associated aggregates, leading to a higher elastic modulus than that of PC3_1 copolymer solution. As a comparison, with the same amount of PNiPAm weight ratio, PS5_1 solution displayed similar rheological trend as that of PC5_1 solution but with a much lower G' around 8 Pa (solid green curve in Fig. 10 (a)), indicating less copolymer aggregations and weaker viscoelastic networks are present in the solution. In Fig. 10 (b), PS3_1 showed a maximum G' around 1 Pa (solid gold curve) and illustrated a subtle sol-gel transition in the temperature range of interest, where there was minimum difference between G' and G'' at 40 °C. Despite different flow procedures, the magnitude of G' and G'' and rheological behaviors of PC3_1 and PS3_1 solutions display the same trend in plots shown in Fig. 9 and Fig. 10.

We propose that different rheological responses in PC and PS based copolymer solution are originated from different thermo-responsive features between sulfobetaine groups in
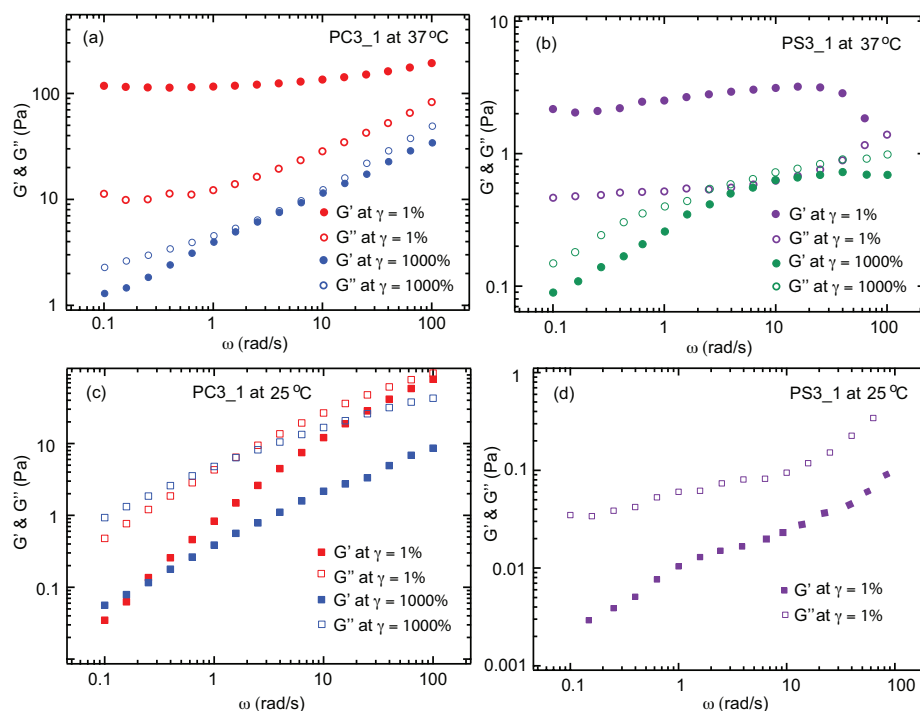
Fig. 9 Elastic modulus G' (filled symbols) and viscous modulus G'' (hollow symbols) for 8 wt% PC3_1 at (a) 37 °C and (c) 25 °C and PS3_1 at (b) 37 °C and (d) 25 °C. Both small ($\gamma = 1\%$) and large ($\gamma = 1000\%$) strains were applied in each figure.

SBMA and carboxyl groups in CBMA. The hydration layers formed by sulfobetaine coils in SBMA increased with elevating temperature and inhibited the formation of associated micellar network, while carboxyl coils in CBMA were less affected. As a result, the blob-coil structures were separated further due to strong hydration layers surrounding SBMA coils at higher temperatures, leading to weakly connected networks. Since CBMA coils were inert to thermal effects, the increasing temperature did not hinder associated micellar aggregates to form stronger elastic networks, see schematics in Fig. 11.

Regarding the chemical structure, there are only 2 carbon chains separating the positively charged group ($N(CH_3)_3^+$) and negative group (COO^-) in CBMA monomers (see Fig. 1). The shorter chains in CBMA allow closely packed ionic pairings between polymer chains, yielding more uniformly packed hydration layers and stronger intermolecular forces compared with SBMA copolymers[3], which has 3 carbons linking the ammonium ($N(CH_3)_3^+$) and the sulfonate group (SO_3^-). For the PC based copolymer, the increasing temperature mainly shrunk the water molecules in PNiPAm chains but exerted minor influence on the binding affinity within CBMA chains, giving rise to a stable associated micellar network. Hence incorporating CBMA with NiPAm provides a tractable and facile way to combine non-fouling feature with thermo-responsiveness, without compromising its mechanical properties.

ties.

3.3.3 Recoverability under alternating amplitude oscillatory shear We examined the elastic behavior of the copolymer gel (PS3_1 and PC3_1) under both mechanical and thermal stimulus, with the emphasis on the recovery response at body temperature 37 °C.

We first alternated small ($\gamma=1\%$, $f= 0.1$ Hz, 10 min) and large strain amplitude oscillations ($\gamma=1000\%$, $f= 0.1$ Hz, 4 min) to both 8 wt% PC3_1 and PS3_1 copolymer solutions at 37 °C. The elastic modulus G' of the solution was plotted as a function of time, see Fig. 12. The G' obtained at small amplitude oscillatory shear measurement ($\gamma=1\%$, $f= 0.1$ Hz) was consistent with the temperature sweep measurement presented in Fig. 10(b): the G' for PC3_1 at 37 °C was 2 orders magnitude higher than that of PS3_1.

The copolymer network generally consists of two types of interactions: covalent bonds between polymer chains, and non-covalent bonds including ionic interactions from zwitterionic groups and hydrogen bonds from hydrophilic chains with water. The dynamics of ionic interactions formed interchain bonds between CBMA ions across the interface and repaired the damage subsequently at smaller strains. At 37 °C, the PC3_1 solution was viscous and it became difficult to rebuild ionic bridges after large strain deformations. The noncovalent bonds in the solution thus cannot be fully recovered at this
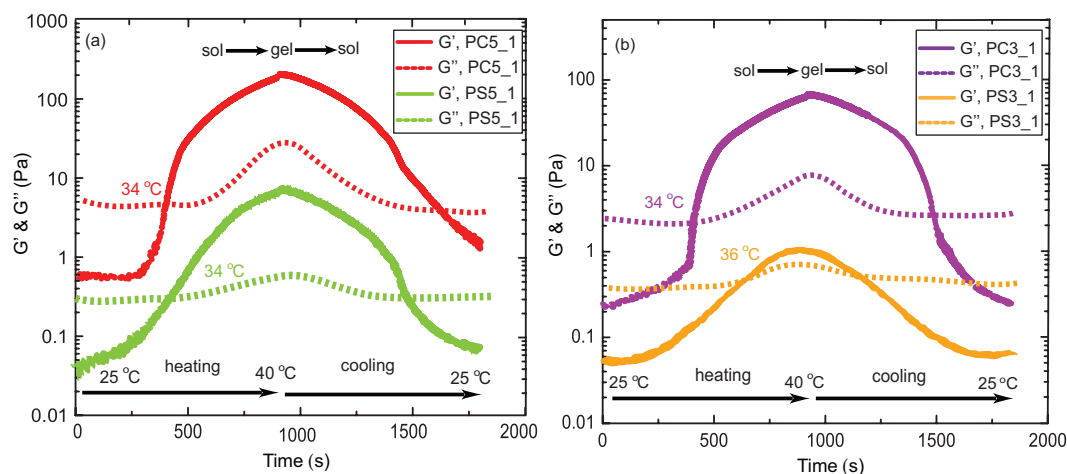
Fig. 10 Elastic modulus G' (solid curves) and viscous modulus G'' (dash curves) for 8 wt% (a) PC5_1 and PS5_1 copolymer solutions (b) PC3_1 and PS3_1 copolymer solutions under small amplitude oscillation ($\gamma = 1\%$ and $f = 0.1$ Hz) from 25 to 40 °C.
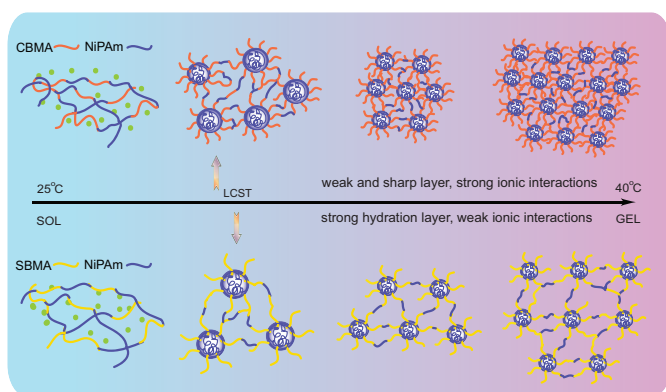

Fig. 11 Strong associated self assembly structures for poly(NiPAm-*co*-CBMA) and weakly associated structures for poly(NiPAm-*co*-SBMA) copolymers with elevating temperature. The temperature axis is not to scale.

stage, showing a decrease of G' at $\gamma = 1\%$ after large amplitude $\gamma = 1000\%$, with $\sim 40\%$ recovery, which, however, is still higher than that of PS3_1 solution under the same condition.

Despite the initial drop of G' under $\gamma = 1000\%$, elastic modulus G' of PC3_1 remained stable and gradually recovered back partially at subsequent strain amplitude cycles (see Fig.12(a)). From the first to the second cycle, the 40% drop of G' originates from the broken non-covalent bonds and deconstructed gel network under large amplitude oscillatory shear, which is similar to "yield-like" behavior observed in colloidal polymer gels: solid to fluid like transtion can occur by varying strains [44–47].

In our system, we also observed similar gel to viscoelastic fluid transition in PC3_1 at 37 °C (see Fig. 9). PC3_1 at 37 °C exhibited typical gel response at $\gamma = 1\%$, with G' being

close to a constant and G'' curve was consistently lower than the G' curve spanning the entire frequency range (red symbols in Fig. 9(a)). At larger strain $\gamma = 1000\%$, PC3_1 showed viscoelastic fluidic response (blue symbols in Fig. 9(a).)

Beyond the second cycle, even though large scale recovery of the gel structure is difficult because non-covalent bonds cannot be fully recovered, dynamic heterogeneities and interactions among small colloidal clusters may occur at smaller length scales and allow a rebound in elasticity. In particular, zwitterions are able to attract each other and bond to smaller clusters [44,45]. Therefore, an overall strengthening of the gel was observed due to bond dominated kinetic arrest [45] subsequent to the second strain cycle. This "in-cage" or inner cluster bonds remained stable as long as thie "cage" remained unbroken. In our case, the G' in the 3rd and 4th cycles were very close but they are smaller than the initial G'.

The recovery argument applied in the PC3_1 was not applicable to PS3_1 with a weak gel network. Once the gel was deconstructed from the first large amplitude oscillatory shear, there wasn't enough attracted colloidal aggregates to induce structure inhomogeneities. Hence, no recovery of G' was observed and the elastic modulus G' for PS3_1 solution decreased an order of magnitude after 4 cycles of alternating strains in the oscillatory shear flows.

In Fig. 13, we measured the elastic modulus of PC3_1 and PS3_1 copolymer solutions by alternating both temperature and oscillatory strain amplitudes. The elastic modulus G' of the solution was plotted as a function of time in the linear viscoelastic regime ($\gamma = 1\%$, $f = 0.1$ Hz, 10 min) before and after a large amplitude oscillation ($\gamma = 1000\%$, $f = 0.1$ Hz, 4 min), under both room temperature (25 °C) and body temperature (37 °C). The sample was initially held at 37 °C, cooled down to 25 °C, then heated back to 37 °C with a temperature ramp
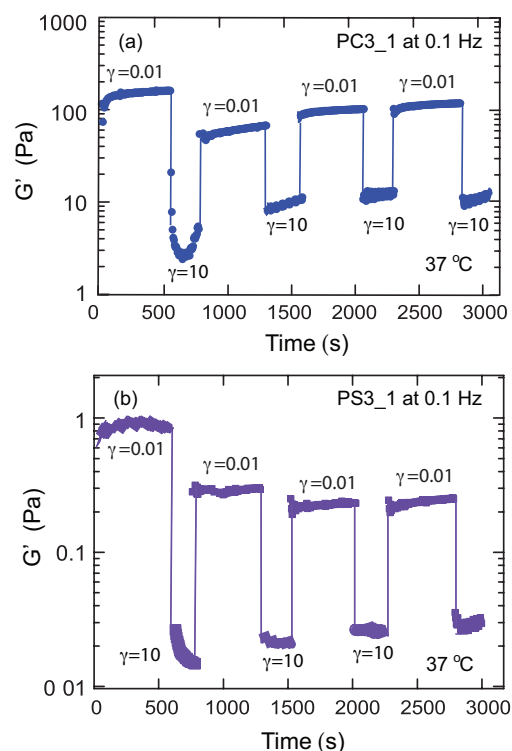
Fig. 12 Elastic moduli G' for 8 wt% (a) PC3_1; (b) PS3_1 copolymer solutions under alternating large and small strain amplitude oscillations at body temperature 37 °C.

varying from 25 to 40 °C. In addition, alternating small and large strain amplitudes were applied during oscillatory shear flow to probe the recoverability of the elastic network in copolymer solutions, at both room and body temperatures. Followed by an initial decrease of G' at large strain 1000%, the elastic modulus G' maintained partial recovery in the subsequent cycles at 37 °C for PC3_1 copolymer solution. Once the temperature was dropped to room temperature (below LCST), a complete recovery of the elastic network was observed, with G' exhibiting the original value, indicating that noncovalent bonds could be rebuilt reversibly with respect to temperature for the PC based copolymer solution. In comparison, PS3_1 copolymer solution showed much weaker viscoelasticity and displayed strong influence under thermal stimulus. In short, the PCBMA chains incorporated with PNiPAm copolymer preserved its viscoelasticity with both thermal and mechanical stimulus.
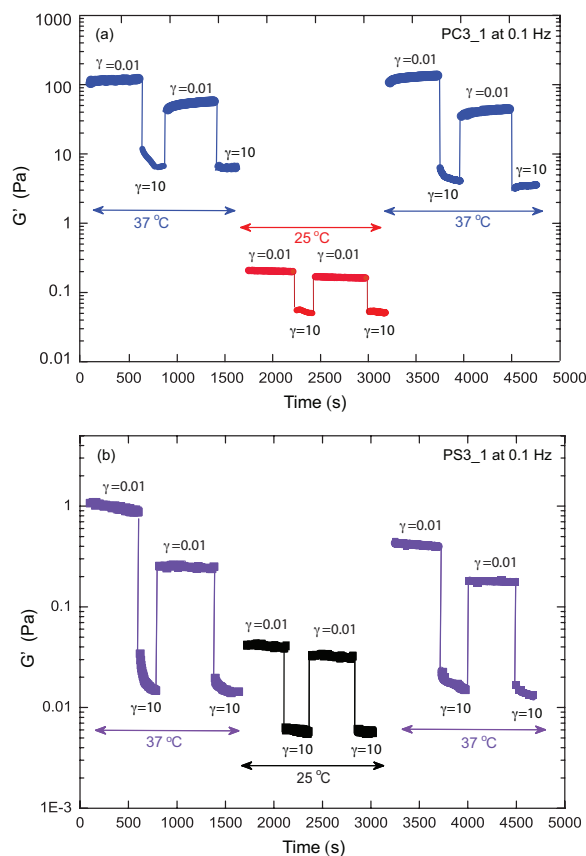
rate of 1 °C/min. Similar to the partial structure recovery observed in Fig. 12, a decreasing trend of G' was observed for the first two cycles of oscillatory shear flow with different strain amplitudes, which was caused by the temporal disassociation of micellar aggregates after large strain deformations. When the temperature was lowed to 25 °C (below LCST), the polymer chains were able to rehydrate to reconstruct with hydrogen bonds. We observed full recovery of $G' \sim 100$ Pa for PC3_1 solution after we raised the temperature back to 37 °C. As a comparison, PS3_1 solution showed weaker G' around 1 Pa at 37 °C and 0.03 Pa at 25 °C (see Fig. 13(b)), indicating that ionic interactions in the PS copolymer were too weak to serve as bridges to form elastic networks. The micelles in PS3_1 were sparsely dispersed due to the strong hydration layers formed around SBMA coils. Therefore, the elastic modulus G' of PS3_1 solution at the second cycle of $\gamma = 1$% was very close to the initial G' in PS3_1 solution at room temperature 25 °C, which was likely due to the breakup and recombination of hydrogen bonds in the co-polymer solution, not related to the elastic recovery.

In summary, systematic rheological characterizations were conducted to evaluate the sol-gel transition behavior for both PC3_1 and PS3_1 copolymer solutions with temperatures

Fig. 13 Elastic moduli G' for 8 wt% (a) PC3_1; (b) PS3_1 copolymer solutions under alternating large and small amplitude oscillations at both room and body temperatures.

4   Conclusions

We compared both thermoresponsive and elastic recovery properties of two different statistical copolymer (poly(NiPAm-*co*-CBMA) and poly(NiPAm-*co*-SBMA)) solutions. We showed that hydrophilic sulfobetaine group present in the PSBMA was strongly influenced by elevating temperatures, which counter affected the thermal properties in the pure PNiPAm based polymer at temperatures higher than its LCST. While carboxybetaine group in PCBMA is weakly affected by temperatures, poly(NiPAm-*co*-CBMA) solution is able to preserve its thermoresponsive nature. In addition, CBMA acted as stronger ionic bridges in poly(NiPAm-*co*-CBMA) to form reinforced elastic networks with superior recovery features when compared with poly(NiPAm-*co*-SBMA). Our work demonstrates that incorporating CBMA in the thermo-responsive PNiPAm provides a tractable and facile way to integrate non-fouling with thermo-responsive features, without compromising its mechanical properties.

5   Acknowledgments

References

1. Y. Chang, S. Chen, Q. Yu, Z. Zhang, M. Bernards and S. Jiang, *Biomacromolecules*, 2006, **8**, 122–127.
2. Z. Zhang, T. Chao, S. Chen and S. Jiang, *Langmuir*, 2006, **22**, 10072–10077.
3. S. Chen and S. Jiang, *Adv. Mater.*, 2008, **20**, 335–338.
4. G. Cheng, L. Mi, Z. Cao, H. Xue, Q. Yu, L. Carr and S. Jiang, *Langmuir*, 2010, **26**, 6883–6886.
5. A. J. Keefe, N. D. Brault and S. Jiang, *Biomacromolecules*, 2012, **13**, 1683–1687.
6. D. A. Herold, K. Keil and D. E. Bruns, *Biochem. Pharmacol.*, 1989, **38**, 73–76.
7. M. Shen, L. Martinson, M. S. Wagner, D. G. Castner, B. D. Ratner and T. A. Horbett, *J. Biomater. Sci., Polym. Ed.*, 2002, **13**, 367–390.
8. V. Gaberc-Porekar, I. Zore, B. Podobnik and V. Menart, *Curr. Opin. Drug. Discov. Devel.*, 2008, **11**, 242–250.
9. J. Ladd, Z. Zhang, S. Chen, J. C. Hower and S. Jiang, *Biomacromolecules*, 2008, **9**, 1357–1361.
10. W. Yang, H. Xue, W. Li, J. Zhang and S. Jiang, *Langmuir*, 2009, **25**, 11911–11916.
11. S. Jiang and Z. Cao, *Adv. Mater.*, 2010, **22**, 920–932.
12. L. Zhang, Z. Cao, T. Bai, L. Carr, J.-R. Ella-Menye, C. Irvin, B. D. Ratner and S. Jiang, *Nat. Biotechnol.*, 2013, **31**, 553–556.
13. Q. Shao, Y. He, A. D. White and S. Jiang, *J. Phys. Chem. B*, 2010, **114**, 16625–16631.
14. H. Schild, *Prog. Polym. Sci.*, 1992, **17**, 163–249.
15. M. D. C. Topp, P. J. Dijkstra, H. Talsma and J. Feijen, *Macromolecules*, 1997, **30**, 8518–8520.
16. C. M. Schilli, M. Zhang, E. Rizzardo, S. H. Thang, Y. K. Chong, K. Edwards, G. Karlsson and A. H. E. Müller, *Macromolecules*, 2004, **37**, 7861–7866.
17. Y. Chang, W. Y. Chen, W. Yandi, Y. J. Shih, W. L. Chu, Y. L. Liu, C. W. Chu, R. C. Ruaan and A. Higuchi, *Biomacromolecules*, 2009, **10**, 2092–2100.
18. R. Pelton, *Adv. Colloid Interface Sci.*, 2000, **85**, 1–33.
19. G. Kali, S. Vavra, K. Làszló and B. Ivàn, *Macromolecules*, 2013, **46**, 5337–5344.
20. C. Wu and X. H. Wang, *Phys. Rev. Lett.*, 1998, **80**, 4092–4094.
21. H. G. Schild and D. A. Tirrell, *J. Phys. Chem.*, 1990, **94**, 4352–4356.
22. J. Virtanen and H. Tenhu, *Macromolecules*, 2000, **33**, 5970–5975.
23. J. Virtanen, M. Arotçaréna, B. Heise, S. Ishaya, A. Laschewsky and H. Tenhu, *Langmuir*, 2002, **18**, 5360–5365.
24. M. J. Kositza, C. Bohne, P. Alexandridis, T. A. Hatton and J. F. Holzwarth, *Langmuir*, 1999, **15**, 322–325.
25. B. J. Chu, *Langmuir*, 1995, **11**, 414–421.
26. E. Alami, M. Almgren, W. Brown and J. Franois, *Macromolecules*, 1996, **29**, 2229–2243.
27. N. P. Shusharina, I. A. Nyrkova and A. R. Khokhlov, *Macromolecules*, 1996, **29**, 3167–3174.
28. K. Skrabania, W. Li and A. Laschewsky, *Macromol. Chem. Phys.*, 2008, **209**, 1389–1403.
29. A. B. Lowe, N. C. Billingham and S. P. Armes, *Macromolecules*, 1998, **31**, 5991–5998.
30. J. Adelsberger, A. Kulkarni, A. Jain, W. Wang, A. M. Bivigou-Koumba, P. Busch, V. Pipich, O. Holderer, T. Hellweg, A. Laschewsky, P. Müller-Buschbaum and C. M. Papadakis, *Macromolecules*, 2010, **43**, 2490–2501.
31. R. Hariharan, C. Biver, J. Mays and W. B. Russel, *Macromolecules*, 1998, **31**, 7506–7513.
32. S. Misra, S. Varanasi and P. P. Varanasi, *Macromolecules*, 1989, **22**, 4173–4179.
33. Y. Maeda, H. Mochiduki and I. Ikeda, *Macromol. Rapid Commun.*, 2004, **25**, year.
34. M. Arotaréna, B. Heise, S. Ishaya and A. Laschewsky, *J. Am. Chem. Soc.*, 2002, **124**, 3787–3793.
35. J. A. Hayward and D. Chapman, *Biomaterials*, 1984, **5**, 135 – 142.
36. K. Ishihara, *Trends Polym. Sci.*, 1997, **5**, 401–407.
37. A. B. Lowe, M. Vamvakaki, M. A. Wassall, L. Wong, N. C. Billingham, S. P. Armes and A. W. Lloyd, *J. Biomed. Mater. Res.*, 2000, **52**, 88–94.
38. A. B. Lowe, N. C. Billingham and S. P. Armes, *Chem. Commun.*, 1996, 1555–1556.
39. Y. Chang, W. Yandi, W. Y. Chen, Y. J. Shih, C. C. Yang, Y. Chang, Q. D. Ling and A. Higuchi, *Biomacromolecules*, 2010, **11**, 1101–1110.
40. F. O. Obiweluozor, A. GhavamiNejad, S. Hashmi, M. Vatankhah-Varnoosfaderani and F. J. Stadler, *Macromol. Chem. Phys.*, 2014, **215**, 1077–1091.
41. D. E. Koppel, *J. Chem. Phys.*, 1972, **57**, 4814–4820.
42. S. W. Provencher, *Biophys. J.*, 1976, **16**, 27–29.
43. S. W. Provencher, *J. Chem. Phys.*, 1976, **64**, 2772–2777.
44. T. Gibaud, D. Frelat and S. Manneville, *Soft Matter*, 2010, **6**, 3482–3488.
45. N. Koumakis and G. Petekidis, *Soft Matter*, 2011, **7**, 2456–2470.
46. J. Sprakel, S. B. Lindström, T. E. Kodger and D. A. Weitz, *Phys. Rev. Lett.*, 2011, **106**, 248303.
47. S. A. Rogers, B. M. Erwin, D. Vlassopoulos and M. Cloitre, *J. Rheol.*, 2011, **55**, 435–458.